COR1-A Pre- and Post-Vibration Tests, May–June 2004

William Thompson

Eric Mentzell

June 25, 2004

This is a report on the results of performance verification measurements made of the COR-1A instrument before and after vibration in early June 2004. The pre-vibration measurements were made on May 28, and the post-vibration measurements were made on June 11. An additional performance verification test was performed on June 16 after the fail-safe door mechanism was tested. All three sets of measurements were made in the COR-1 clean room facility in Building 5.

1 Exposure time test

The pre-vibration results of the exposure time test were previously reported in the COR-1A final assembly report.

The procedure EXPTIMETEST takes a series of exposures ranging from 0.1 to 10 seconds, together with the associated dark images. Intercomparing the resulting images allows the accuracy of the exposure times to be explored. To keep the instrument from saturating at the longer exposure times, the lamp current was reduced from 6 to 4 amps. Even so, some saturation occured at the longest exposure times due to dark current in the room temperature CCD.

Two keywords in the FITS headers are related to the exposure times. The keyword EXPCMD contains the commanded exposure time, while EXPTIME contains the measured exposure time, based on the motion of the shutter mechanism. For dark images, EXPTIME is calculated using a different algorithm, and is not reliable. Figure 1 shows the difference between the measured and commanded exposure times. The post-vibration and post-door-test results are essentially identical to the pre-vibration measurements.

Figure 2 shows the relationship between the exposure time and the measured signal in the detector. The behavior of all three data sets are the same, and differ only in that the lamp brightness was not the same between the two tests.

2 Focus

To measure the instrument resolution, an Air Force 1951 resolution test target was placed at the eyepiece location of a Meade telescope. To take the difference between nitrogen and vacuum focus into account, the target was moved back by a measured distance from the Meade's infinity focus.

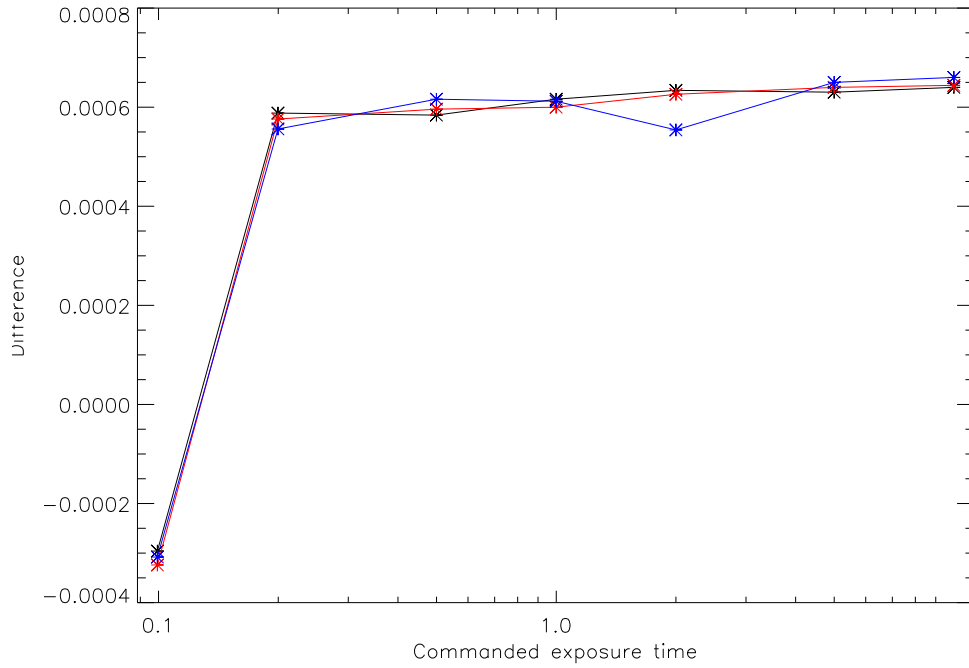Measurements were made at the following six locations on the detector, relative to the center of the CCD:

Figure 1: Difference between measured and commanded exposure times. Black: pre-vibration, red: post-vibration, blue: post-door-test.
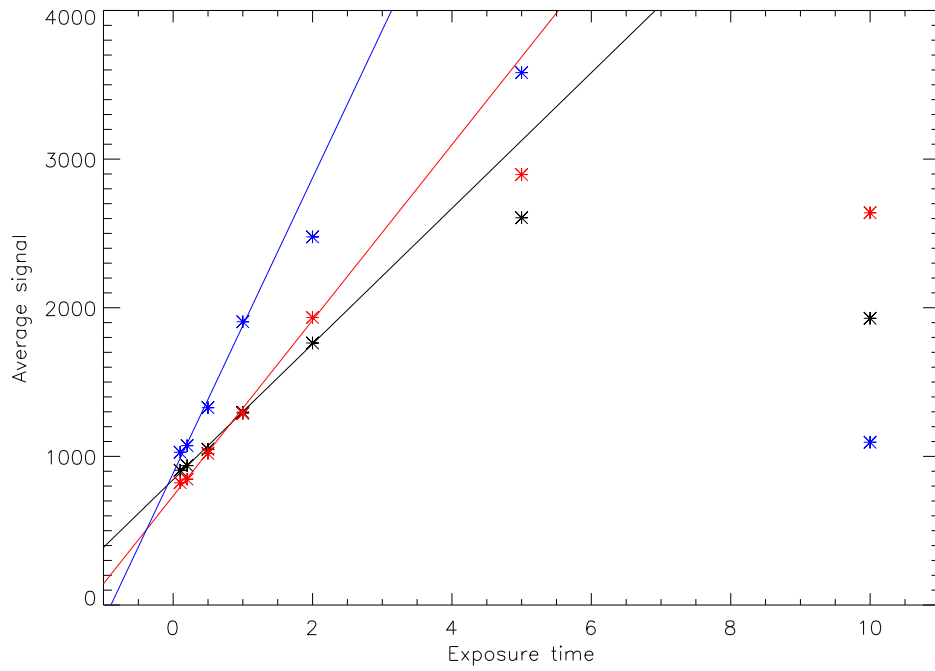

Figure 2: Comparison between measured signal and exposure time. The longer exposure times are affected by saturation in the detector. Black: pre-vibration, red: post-vibration, blue: post-door-test.
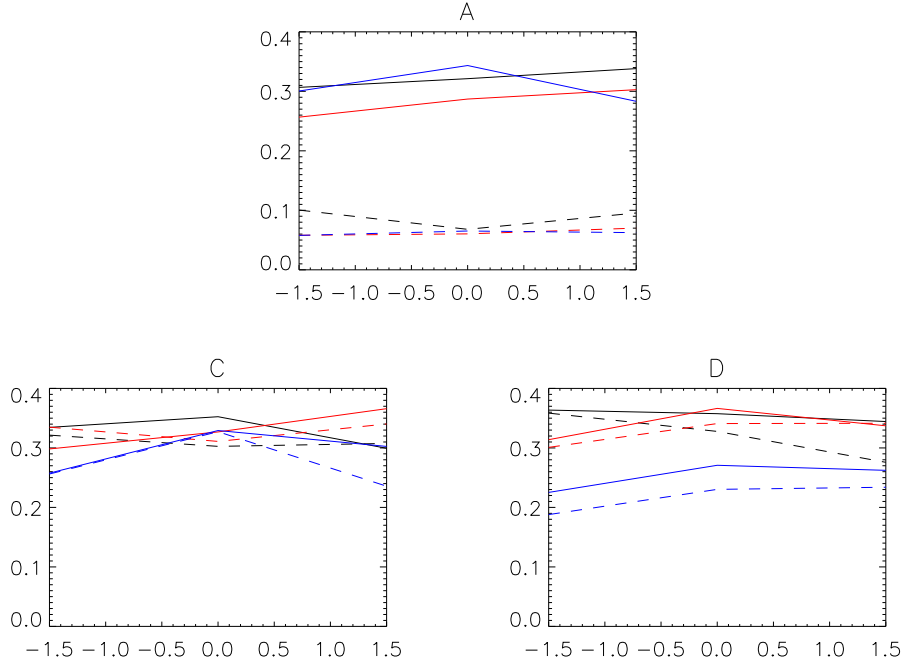
Figure 3: Contrast values as a function of Meade focus for several positions on the detector. Solid lines are for vertical bars, dashed for horizontal bars, black for pre-vibration, red for post-vibration, blue for post-door-test.

Location	X (mm)	Y (mm)
A	0	7.1
C	-5	-5
D	5	-5

At each of the above points, measurements were made at 3 focus positions on the Meade telescope, centered around the nominal position of 8.42 mm, and at ± 1.5 mm. Unlike the final assembly measurements, all the points were done with the Meade telescope in one location. Point D showed some vignetting, but not in the area being measured. Figure 3 shows the results. The results for point A are worse than the measurements made as part of the final assembly testing, and are probably affected by the positioning of the Meade telescope. The pre- and post-vibration results are essentially the same, within the measurement noise, and the uncertainty in the positioning. The post-door-test results at point D are significantly worse than the other measurements. However, this position is visibly affected by vignetting. The most trustworthy measurement point is C, where no changes are seen.

3 Polarizer wedge

Measurements of the Air Force resolution target, made every $15°$, can be used to derive the amount of image motion as a function of polarizer position. The post-vibration measurements show that the target image makes a small circular motion with a radius of 0.27 pixels (3.7 μm, 1.0 arcsec),

and a phase angle of 165°.5. This compares very well with the measurements made as part of the final assembly. The measurements made just before vibration are too noisy to yield a solution. The measurements made after the door test yield a solution of 0.28 pixels and a phase angle of 155°.5. Within the errors of the test, these results are unchanged.

4 Light leak testing

To see if there were any light leaks in the instrument, a series of exposures were taken with a bright flashlight shone on the interface between each tube section, on the FPA mount plate, and on each Mott filter. No light leaks were seen.

A separate test was made of the light tightness of the shutter by taking regular and dark images with the lamp turned on and then turned off. A difference was seen between the two dark images of about 10 DN. This difference image looked exactly like the first image in the sequence, including the bleeding signatures. Obviously, a faint signal of only 10 DN is not going to cause massive bleeding on the detector. Thus, the interpretation is that the first dark image included a faint residual of the previous image.

5 Boresight

The following table gives the theodolite offset from the main reference cube (MRC) $-Z$ cube face to the boresight axis, front illuminated with halo light.

	Δ Azimuth	Δ Elevation
5/27/04 Pre-Vibe	$-00°07'20''$	$+00°02'36''$
6/14/04 Post-Vibe	$-00°07'32''$	$+00°02'39''$
6/15/04 Post-door-test	$-00°07'48''$	$+00°02'58''$

Based on earlier error bar estimates of $9''$ azimuth and $7''$ elevation, these data indicate that nothing moved during the vibration test. The situation after the door test is less clear. However, a separate set of measurements made by Sam Hetherington do not show any significant changes in the boresight. Those results, reported separately, are summarized here.

	Δ Azimuth	Δ Elevation
6/14/04 Post-Vibe	$-00°07'23''$	$+00°02'48''$
6/15/04 Post-door-test	$-00°07'25''$	$+00°02'48''$

6 Flat field test

In order to intercompare the flat fields taken on different dates, a linear scaling needs to be applied to the images to account for the different light levels, and the different amounts of thermal noise. Figure 4 demonstrates the success of registering the brightness of one image relative to another.

Figure 5 shows the relative differences between the flat field images, normalized to the average unvignetted signal. The image on the left is the difference between the pre- and post-vibration
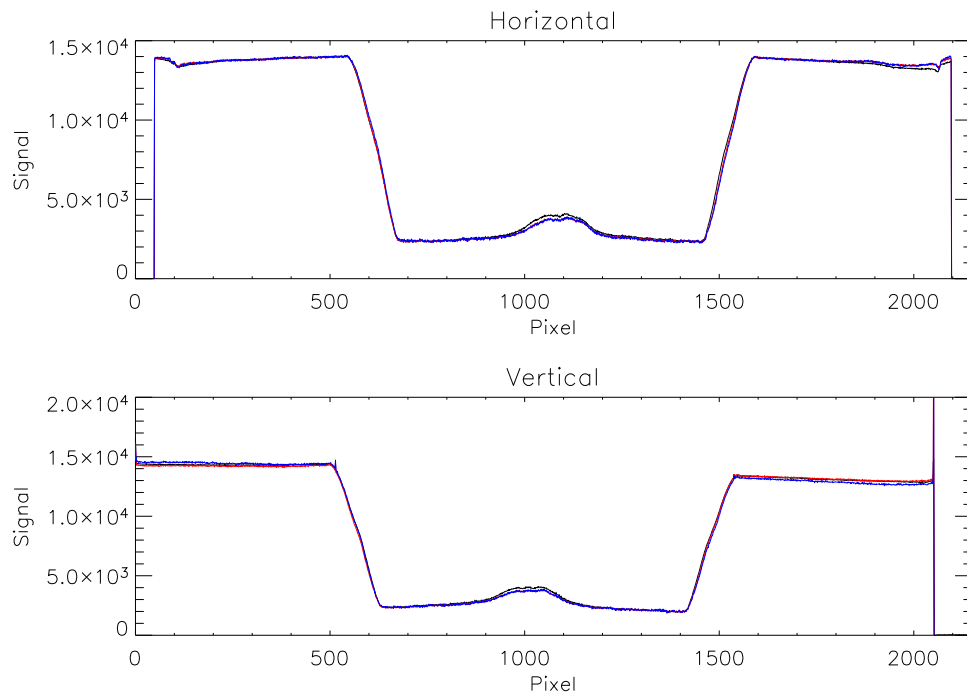
Figure 4: Comparison of horizontal and vertical traces through the flat field images. Black: pre-vibration, red: post-vibration, blue: post-door-test.
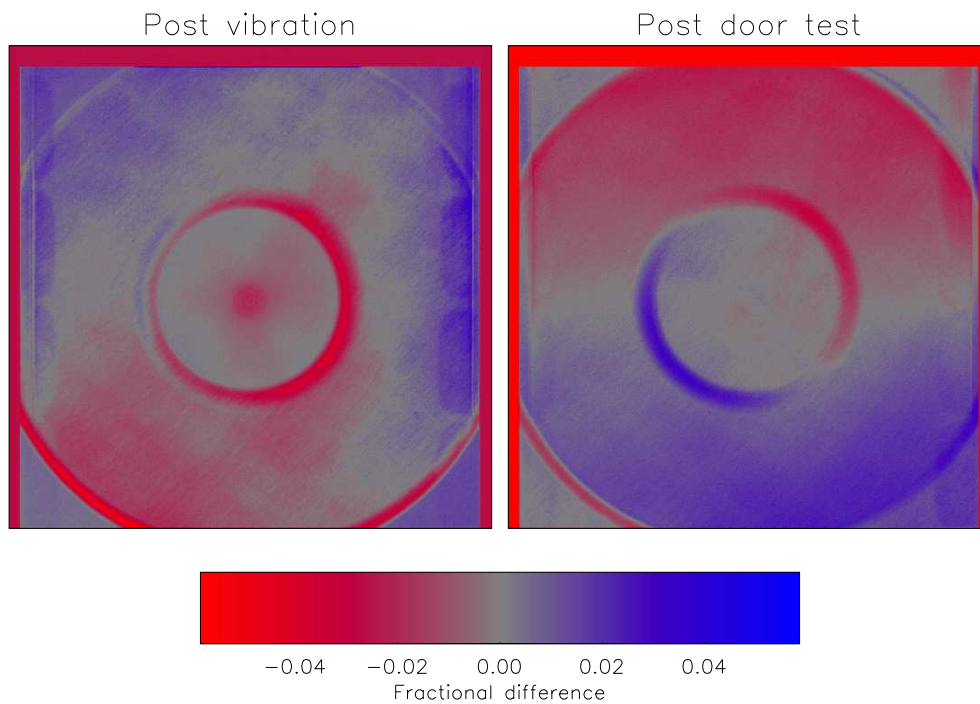

Figure 5: Relative differences between flat field images, normalized to the average unvignetted signal. Left: post-vibration minus pre-vibration, right: post-door-test minus post-vibration.

measurements. There's evidently a difference in the amount of scattered light, as evidenced by the fact that the central dot is brighter in the pre-vibration data. This difference in the ratio of the scattered light to the direct flat field light may be affecting the accuracy of the linear scaling of one image to the other, which may be why the penumbral region appears fainter all the way around the mask after vibration. There is an asymmetry, though, with the right side difference more negative than the left side, with even some positive difference on the left side. The large scale features are due to thermal effects.

On the right side of Figure 5 is the difference between the measurements made after the door test, subtracted by the measurements made after vibration. There's a distinct difference within the mask penumbra, with positive differences on one side of the mask, and negative differences on the other side. Note that there's no signature of the diffuse spot in the center of the mask shadow, which means that this did not change after the door test. There's also a general trend from top to bottom, which is probably a thermal effect.

To more precisely track the changes in the flat field, polynomial fits were made of the penumbral region. The procedure was as follows

1. Make a series of traces through the penumbral region every $10°$ from a selected point reasonably close to the center of the occulter shadow.

2. For each trace, determine the signal representing completely closed and completely open, and rescale the trace to run between 0 and 1.

3. Make a polynomial fit of the form

$$r = a_0 + a_1 I + a_2 I^2 \tag{1}$$

   where r is the pixel position, and I is the rescaled brightness. Note that this is opposite (sideways) of the normal way of fitting a polynomial.

The procedure is demonstrated in Figure 6 for a representative sample trace through one of the flat field images.

Figure 7 shows the results of fitting Eq. 1 to the flat field images. The angle is measured counter-clockwise from the x (i.e. rightwards) axis. The top two plots show the extrapolations of the curves to $y = 0$ and $y = 1$, which are closely associated with the edges of the penumbra. The other two plots show the shape parameters a_1 and a_2. From these plots can be deduced the following:

- After vibration, small changes were seen in the position, size, and shape of the occulter shadow.

- The total amount of shift after vibration is ∼1 pixel. This is interpreted as a relative motion between the focal plane mask and the CCD.

- The changes in size seen after vibration, also ∼1 pixel, may be related to the difference in the relative amount of scattered light within the mask shadow.

- The inner and outer edges of the penumbra do not move after the door test, i.e. the relationship between the focal plane mask and the CCD did not change.
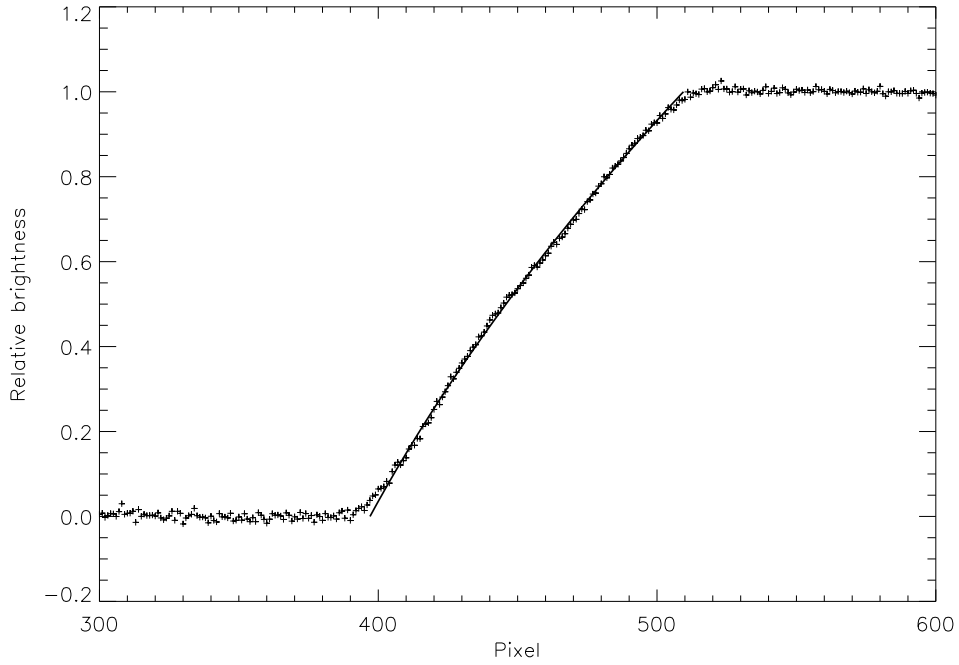
Figure 6: Demonstration of fitting Eq. 1 to a normalized penumbral shadow.

- Models show that there is a very distinct signature when the occulter is misaligned sufficiently to come out from behind the focal plane mask. This signature is very strong, and is spatially confined to just outside the inner penumbral edge. This signature is not seen in the data.

- The variation in the slope a_1 in Figure 7 is the inverse of the variation in the second order parameter a_2. This reflects the fact that the width of the penumbra does not change.

- The differences seen in Figure 5 before and after the door test are due to the change in the shape of the penumbra, and do not reflect a motion of either the focal plane mask or occulter.

The significance of the subtle changes in curvature of the penumbra is still under investigation. However, nothing in the flat field images suggest that any problems devloped during either the vibration test or the door test.
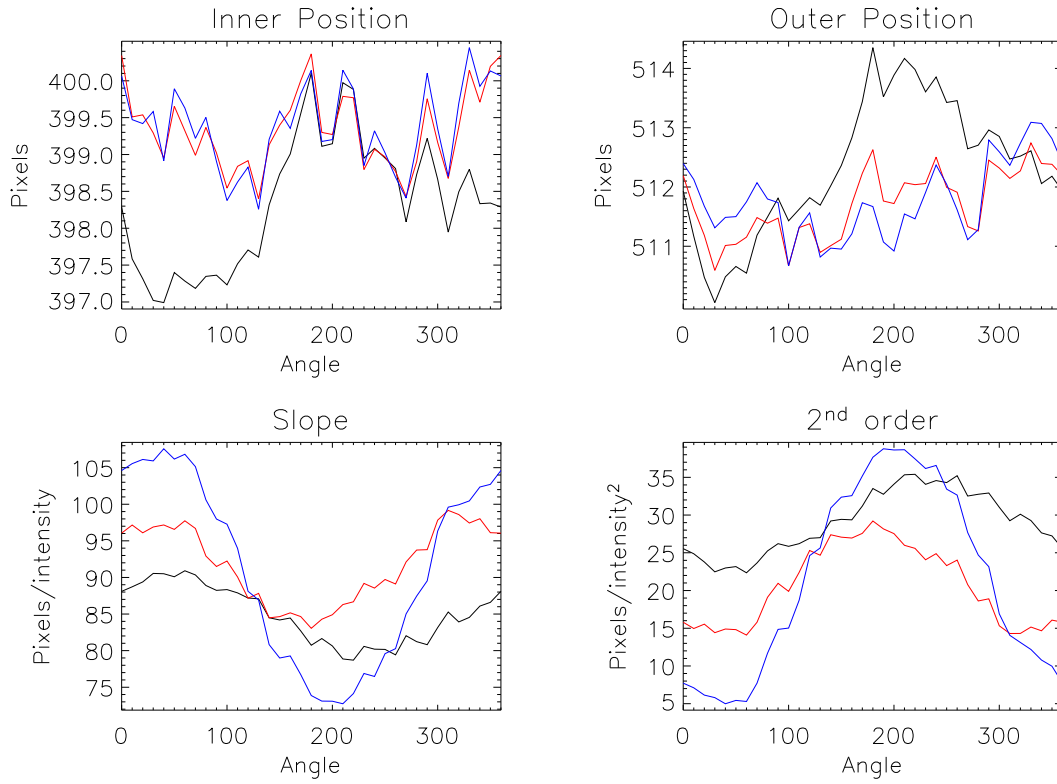
Figure 7: Results of fitting Eq. 1 to the flat field images. The top two plots show the extrapolations of the curves to $y = 0$ and $y = 1$, which represent the inner and outer edges of the penumbra. The bottom two plots show the parameters a_1 and a_2 respectively. Black: pre-vibration, red: post-vibration, blue: post-door-test.